Effect of Structural Supermodulation on Superconductivity in Trilayer Cuprate $Bi_2Sr_2Ca_2Cu_3O_{10+\delta}$

Changwei Zou,[1,*] Zhenqi Hao,[1,*] Haiwei Li,[1] Xintong Li,[1] Shusen Ye,[1] Li Yu,[2] Chengtian Lin,[3] and Yayu Wang[1,4,†]
[1]State Key Laboratory of Low Dimensional Quantum Physics, Department of Physics, Tsinghua University, Beijing 100084, People's Republic of China
[2]Beijing National Laboratory for Condensed Matter Physics, Institute of Physics, Chinese Academy of Sciences, Beijing 100190, People's Republic of China
[3]Max Planck Institute for Solid State Research, Heisenbergstrasse 1, D-70569 Stuttgart, Germany
[4]Frontier Science Center for Quantum Information, Beijing 100084, People's Republic of China

(Received 29 April 2019; revised manuscript received 24 July 2019; published 31 January 2020)

We investigate the spatial and doping evolutions of the superconducting properties of trilayer cuprate $Bi_2Sr_2Ca_2Cu_3O_{10+\delta}$ by using scanning tunneling microscopy and spectroscopy. Both the superconducting coherence peak and gap size exhibit periodic variations with structural supermodulation, but the effect is much more pronounced in the underdoped regime than at optimal doping. Moreover, a new type of tunneling spectrum characterized by two superconducting gaps emerges with increasing doping, and the two-gap features also correlate with the supermodulation. We propose that the interaction between the inequivalent outer and inner CuO_2 planes is responsible for these novel features that are unique to trilayer cuprates.

DOI: 10.1103/PhysRevLett.124.047003

Although the mechanism of superconductivity in cuprates is still elusive, there are empirical rules that put strong constraints on the theoretical models. A well-established trend is that, for the same cuprate family, the maximum transition temperature (T_c) increases with the number of CuO_2 planes in each unit cell up to the trilayer limit [1]. Trilayer cuprates not only have the highest T_c, but also have the unique situation with two types of inequivalent CuO_2 planes. As shown by the schematic crystal structure in Fig. 1(a), the inner CuO_2 plane (IP) is sandwiched between two outer planes (OPs) and may have distinct electronic structures. It is expected that the IP has a lower carrier density and larger pairing potential, whereas the OP has a higher carrier density and stronger phase rigidity [2]. The cooperation of these two factors is proposed to be beneficial for optimizing the superconductivity [3]. However, there is still a debate regarding how the two types of CuO_2 layers couple with each other, whether through the single-particle proximity effect [4] or the Josephson tunneling of Cooper pairs [5].

The $Bi_2Sr_2Ca_2Cu_3O_{10+\delta}$ (Bi-2223) compound has attracted particular attention, because it is ideal for surface-sensitive probes such as angle-resolved photoemission spectroscopy (ARPES) [6,7] and scanning tunneling microscopy (STM) [8,9]. ARPES experiments on Bi-2223 have revealed the existence of two bands originated from the IP and OP, respectively [10,11]. Another interesting issue in Bi-family cuprates is the existence of structural "supermodulation," which causes dramatic distortions from the flat crystalline planes. Although it is usually considered as a nuisance in data analysis, from a more optimistic perspective it provides a new knob for perturbing the CuO_2 planes. STM experiments on double-layer $Bi_2Sr_2CaCu_2O_{8+\delta}$ (Bi-2212) have revealed a periodic variation of the superconducting (SC) gap size with supermodulation [12], but a similar study in Bi-2223 is still lacking. The response of Cooper pairs to the lattice distortion within each CuO_2 plane, plus the interaction between the IP and OP, may provide unique clues about the origin of superconductivity.

In this Letter, we use STM to investigate the effect of structural supermodulation on superconductivity in Bi-2223. Both the SC coherence peak height and gap size exhibit periodic variations with supermodulation, but the effect is much more pronounced in the underdoped regime than at optimal doping (OPT). Moreover, a new type of spectrum with two SC gaps emerges with increasing doping, and its features also correlate with the supermodulation. We propose that the intricate interaction between the IP and OP is responsible for these novel features in trilayer cuprates.

The Bi-2223 single crystals are grown by the traveling solvent floating zone method and are postannealed in mixed Ar and O_2 gas flow to control the doping level [13,14]. The single crystal is cleaved *in situ* at room temperature and is then transferred into the STM system working at 5 K. A tungsten tip is treated and calibrated on an Au(111) surface before the measurement, as described previously [15]. The dI/dV differential conductance, which is approximately proportional to the density of state, is obtained by the ac lock-in method with modulation frequency $f = 573$ Hz.

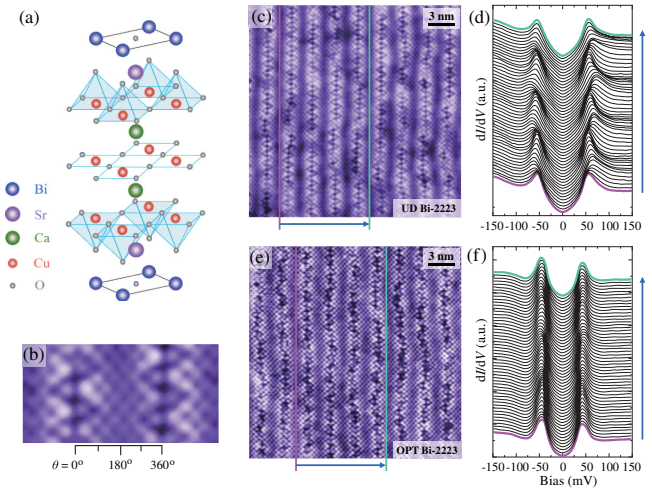

FIG. 1. (a) Schematic half-unit-cell crystal structure of Bi-2223. (b) Illustration of the spatial phase θ of supermodulation. (c) Topographic image (24×24 nm^2) and (d) spatial variation of tunneling spectra of an underdoped (UD) Bi-2223, where the blue arrows indicate the direction along which the spectra are displayed. (e),(f) The same plots for an OPT Bi-2223 sample. The topographic images in (c) and (e) are taken with bias voltage $V = -250$ mV and tunneling current $I = 10$ pA and $I = 40$ pA, respectively.

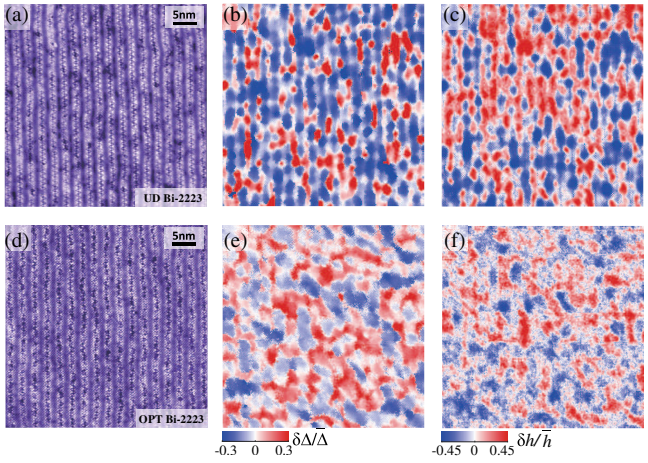

FIG. 2. The topographic image (a), the spatial distribution of relative gap size variation (b), and coherence peak height variation (c) of the underdoped Bi-2223 extracted from the spectral grid. (d)–(f) The same set of maps in the OPT Bi-2223. The underdoped sample exhibits much more pronounced periodic variations with the supermodulation than the optimally doped sample.

Figure 1(c) displays the topography of an underdoped Bi-2223 with $T_c^{\text{onset}} \sim 110$ K. Both the atomic lattice of the exposed BiO surface and the supermodulation with ~2.6 nm periodicity can be clearly resolved. In an enlarged image in Fig. 1(b), we assign a spatial phase θ to facilitate data analysis and discussion [12]. The supermodulation ridge and valley correspond to $\theta = 0°$ and 180°, respectively. To reveal the electronic structure of a particular location (or θ value), 128 dI/dV curves are taken along a line parallel to the supermodulation [such as the magenta line in Fig. 1(c)]. The averaged spectra are displayed in Fig. 1(d) with a vertical offset for clarity. There exist strong periodic variations of the dI/dV curves with supermodulation, where the spectra at the valley have a much sharper SC coherence peak and smaller SC gap compared to that at the ridge.

We performed the same measurements on an OPT Bi-2223 with $T_c^{\text{onset}} \sim 113$ K. It is known that the T_c of Bi-2223 is not sensitive to hole concentration [14,16], possibly due to the distinct doping evolution and interplay between the IP and OP [17]. The topography in Fig. 1(e) is similar to the underdoped sample, but the spatially dependent dI/dV curves in Fig. 1(f) show much weaker periodic variations with supermodulation. The overall gap size of the OPT sample, defined as the energy between the Fermi level and coherence peak, is around 45 meV. It is significantly smaller than that of the underdoped sample with $\Delta \sim 67$ meV, which confirms the increase of hole density.

To visualize the spatial patterns of superconductivity, we perform spectroscopic imaging on the underdoped Bi-2223. Figure 2(a) shows the topography of an area where dI/dV curves are taken on a dense grid. In Figs. 2(b) and 2(c), we display the spatial information of SC gap size $\Delta(\mathbf{r})$ and coherence peak height $h(\mathbf{r})$ extracted from the spectral grid. Both quantities are shown as the relative difference to their mean values, i.e., $\delta\Delta/\bar{\Delta} = [\Delta(\mathbf{r}) - \bar{\Delta}]/\bar{\Delta}$ and $\delta h/\bar{h} = [h(\mathbf{r}) - \bar{h}]/\bar{h}$. Despite the existence of inhomogeneities [18,19], there are evident vertical stripy features demonstrating the periodic distribution of the two quantities. The periodicity is exactly the same as the structural supermodulation (see Supplemental Fig. S1 [20]), and the valley shows a smaller SC gap and sharper coherence peak. Because $\Delta(\mathbf{r})$ indicates the pairing strength and $h(\mathbf{r})$ is proportional to the superfluid density [21], these results suggest that supermodulation has a strong influence on the two key factors in underdoped Bi-2223. The same set of data for the OPT Bi-2223 is shown in Figs. 2(d)–2(f). Although there are still faint vertical streaks in the $\Delta(\mathbf{r})$ and $h(\mathbf{r})$ maps, their correlation to the structural supermodulation is much less obvious than that in the underdoped sample.

In Fig. 3(a), we compare the dI/dV spectra at the centers of the supermodulation ridge and valley averaged over the grid. The spectral difference in the underdoped sample is very pronounced, whereas that in the OPT sample is rather weak. In Fig. 3(b), the normalized gap amplitude and coherence peak height in the two Bi-2223 samples are plotted as a function of θ. All data can be fit by a cosine function, and the peak-to-peak amplitudes of the underdoped Bi-2223 are ~25% and ~38% for $\Delta(\mathbf{r})$ and $h(\mathbf{r})$, respectively. In contrast, in the OPT sample, the peak-to-peak variations of $\Delta(\mathbf{r})$ and $h(\mathbf{r})$ are merely ~5% and ~8%,

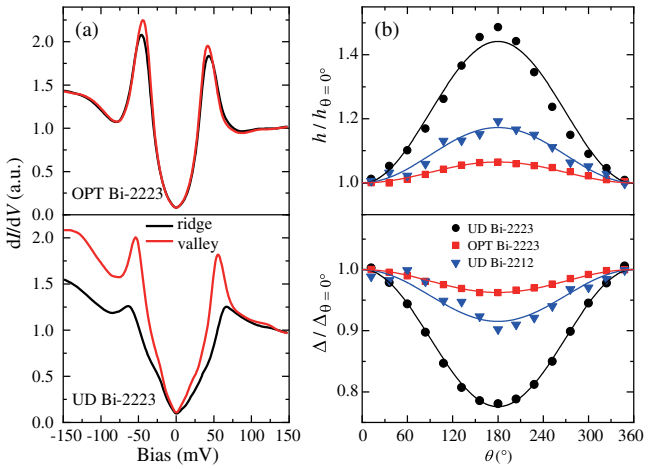

FIG. 3. (a) Averaged dI/dV curves on the supermodulation ridge and valley in UD (lower panel) and OPT (upper panel) Bi-2223, normalized to the background conductance $dI/dV(+135\ \mathrm{mV})$. (b) Normalized gap size (lower panel) and coherence peak height (upper panel) of three different samples as a function of θ. The solid symbols are experimental data, and the curves are fittings by a cosine function.

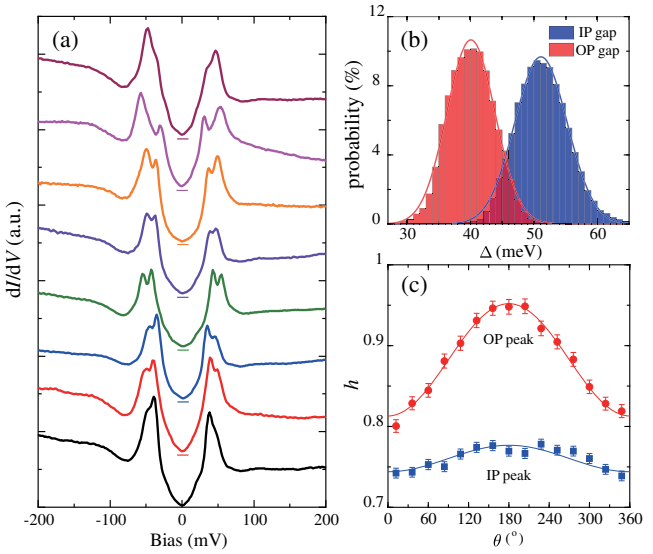

FIG. 4. Emergence of two SC gaps in OPT Bi-2223. (a) Eight representative dI/dV curves showing two SC gaps. Although most spectra show the two-gap feature, the spatial average of them tends to smear it out and leads to a broad peak as shown in Figs. 1(f) and 3(a) (see Supplemental Fig. S5 [20] for details). (b) Histogram of the larger IP gap (blue) and smaller OP gap (red), which can be fit by Gaussian functions (the solid lines) that peak at $\Delta_{\mathrm{OP}} = 40$ meV and $\Delta_{\mathrm{IP}} = 52$ meV, respectively. (c) Peak heights of the fitted double Lorentzian curves as a function of θ. The red and blue curves are cosine fittings of the statistical data.

respectively. The same quantities of a slightly underdoped Bi-2212 are plotted as blue triangles (see Supplemental Fig. S2 [20] for raw data). The amplitudes are ~9% and ~15%, consistent with a previous report [12], and lie between the two Bi-2223 samples. In Supplemental Sec. C [20], we show that the periodic variations are caused by the structural supermodulation instead of the oxygen defects, which can also enhance local Δ [22], settling a long-standing puzzle [23].

Another new feature is the emergence of two SC gaps in the dI/dV of OPT Bi-2223, which are rarely seen in the underdoped sample. The two-gap feature is presumably from the two Fermi surfaces of the IP and OP as probed by ARPES [10,11] and the point contact technique [24]. About 75% of the spectra exhibit two gaps, and Fig. 4(a) shows eight representative dI/dV curves with two coherence peaks in a nearly particle-hole-symmetric manner. To extract the two gaps, we fit each spectrum by using two Lorentzian functions after subtracting the background (see Supplemental Sec. D [20]). The histogram in Fig. 4(b) summarizes the distribution of the two gap sizes, both exhibiting Gaussian line shapes around 40 and 52 meV, respectively. These values are close to the two average gap sizes of 43 and 60 meV observed by ARPES in OPT Bi-2223 [10]. Therefore, the small (large) gap can be ascribed to the OP (IP), respectively [25]. Figure 4(c) plots the fitted peak height $h(\mathbf{r})$ of each gap as a function of θ, both showing cosine dependence with supermodulation. The OP gap has a higher coherence peak, presumably due to a larger superfluid density, and shows stronger spatial variation (peak-to-peak amplitude ~14%) than the IP (~4%).

There are several theories about the effect of supermodulation on superconductivity in Bi-based cuprates. A number of structural factors may give rise to such phenomenon, especially the strong lattice imperfections on the ridge. First, the displacement of apical oxygen and distortion of the CuO_5 pyramid are most severe on the ridge [26], which can enhance the SC gap size due to locally maximized pairing strength [27–29]. Moreover, on the ridge the distance between the apical oxygen and the underneath Cu atom is smaller [26,30], which can enhance the pairing gap through the nearest-neighbor "superrepulsion" [31] or covalency between Cu-3d_{x2-y2} and O-2p_z orbitals [32]. The smaller distance also reduces the SC phase ordering due to delocalization of the Cu-4s orbital and smaller intralayer hopping range [33]. From the charge doping viewpoint, the "Bi-dilute" ridge strongly affects the Sr sites, replacing Sr^{2+} by Bi^{3+}, thus doping electrons [26,34]. The reduced hole density at the ridge also leads to a larger SC gap size and weaker phase coherence. Therefore, the periodic distribution of Δ is triggered by the relationship between the CuO_2 plane and charge reservoir layer, which may induce a spatially dependent pairing potential $V_\theta \sim V_0 + \delta V \cos(\theta)$ [27].

However, none of these factors can explain why underdoped Bi-2223 responds much more strongly to the supermodulation than the OPT sample. Such doping dependence is absent in Bi-2212 [12], suggesting that it is unique to

trilayer Bi-2223 due to the additional IP. Because there was no theoretical discussion about this behavior, here we present only a phenomenological picture. Because the STEM images in Supplemental Fig. S6 [20] reveal that the crystal structure has no observable difference between OPT and underdoped Bi-2223, the key factor should be the decrease of hole doping. The IP of trilayer cuprates is known to have a lower doping level than the OP [10,35,36], and it has been proposed that T_c could be enhanced through the single-electron proximity effect between the underdoped CuO_2 plane with a large pairing potential and the overdoped CuO_2 plane with strong phase stiffness [3,4,37,38]. In underdoped Bi-2223, the severely underdoped IP acts as the "pairing" component [37] and enhances the pairing potential V in the "metallic" OP by V_{IP} [37]. The proximity effect is supported by the SC gap size of ~ 67 meV in the underdoped Bi-2223, contributed by the overdoped OP, which is much larger than that in Bi-2212 with similar doping [39]. Because the relationship between gap size Δ and pairing potential V should be highly nonlinear (e.g., in the weak-coupling BCS framework $\Delta = 2\hbar\omega_c e^{-1/N(0)V}$), an equal enhancement of the pairing strength on the ridge and valley could lead to a strongly different gap size change. As shown in Supplemental Fig. S7 [20], in underdoped Bi-2223 the modulation of the gap size exhibits a strong spatial modulation because $\Delta[V_\theta(0°) + V_{\mathrm{IP}}] \gg \Delta[V_\theta(180°) + V_{\mathrm{IP}}]$, so that the ridge has a much larger gap size than the valley. This is the origin of the strongly enhanced periodic variation of Δ.

Upon reaching optimal doping, the IP is doped with sufficient holes and becomes SC [36], as manifested by the two SC gaps. Now the single-electron proximity effect becomes negligible [17]. The effect of supermodulation is mainly acted on the OP by neighboring apical oxygen, similar to that in Bi-2212. Therefore, the 14% relative variation of the OP coherence peak in Fig. 4(c) is close to the 15% value of Bi-2212. Because the IP is sandwiched between two OPs, the influence of the supermodulation is significantly reduced. The IP lives in a relatively homogeneous environment [35], and its coherence peak variation is merely 4%. Roughly speaking, the response of OPT Bi-2223 to the supermodulation is an average of the two SC planes, and the coherence peak variation of 9% in Fig. 3(b) indeed lies between that of the two individual planes.

In conclusion, STM studies on Bi-2223 reveal the peculiar spatial and doping evolution of superconductivity, which can be explained by the critical role played by the unique inner CuO_2 plane. In the underdoped regime, the IP couples with the OP via the single-electron proximity effect, whereas in the optimally doped regime the IP couples with the OP via Josephson tunneling of Cooper pairs. The distinct doping evolution of the two inequivalent CuO_2 planes and the intricate interplay between them are crucial for understanding the phase diagram of trilayer cuprates, as well as the highest T_c.

We thank Yuan Yao for carrying out the STEM measurements. This work was supported by the MOST of China Grant No. 2017YFA0302900, the NSFC Grant No. 11534007, and the Basic Science Center Project of NSFC under Grant No. 51788104. This work is supported in part by the Beijing Advanced Innovation Center for Future Chip (ICFC).

*These authors contributed equally to this work.
†yayuwang@tsinghua.edu.cn

[1] M. Di Stasio, K. A. Müller, and L. Pietronero, Nonhomogeneous Charge Distribution in Layered High-T_c Superconductors, Phys. Rev. Lett. **64**, 2827 (1990).
[2] H. Kotegawa, Y. Tokunaga, K. Ishida, G.-q. Zheng, Y. Kitaoka, H. Kito, A. Iyo, K. Tokiwa, T. Watanabe, and H. Ihara, Unusual magnetic and superconducting characteristics in multilayered high-T_c cuprates: ^{63}Cu NMR study, Phys. Rev. B **64**, 064515 (2001).
[3] S. A. Kivelson, Making high T_c higher: A theoretical proposal, Physica (Amsterdam) **318B**, 61 (2002).
[4] S. Okamoto and T. A. Maier, Enhanced Superconductivity in Superlattices of High-T_c Cuprates, Phys. Rev. Lett. **101**, 156401 (2008).
[5] S. Chakravarty, H. Y. Kee, and K. Volker, An explanation for a universality of transition temperatures in families of copper oxide superconductors, Nature (London) **428**, 53 (2004).
[6] D. L. Feng, A. Damascelli, K. M. Shen, N. Motoyama, D. H. Lu *et al.*, Electronic Structure of the Trilayer Cuprate Superconductor $Bi_2Sr_2Ca_2Cu_3O_{10+\delta}$, Phys. Rev. Lett. **88**, 107001 (2002).
[7] H. Matsui, T. Sato, T. Takahashi, S. C. Wang, H. B. Yang, H. Ding, T. Fujii, T. Watanabe, and A. Matsuda, BCS-like Bogoliubov Quasiparticles in High-T_c Superconductors Observed by Angle-Resolved Photoemission Spectroscopy, Phys. Rev. Lett. **90**, 217002 (2003).
[8] G. Levy de Castro, C. Berthod, A. Piriou, E. Giannini, and O. Fischer, Preeminent Role of the Van Hove Singularity in the Strong-Coupling Analysis of Scanning Tunneling Spectroscopy for Two-Dimensional Cuprate Superconductors, Phys. Rev. Lett. **101**, 267004 (2008).
[9] N. Jenkins, Y. Fasano, C. Berthod, I. Maggio-Aprile, A. Piriou, E. Giannini, B. W. Hoogenboom, C. Hess, T. Cren, and Ø. Fischer, Imaging the Essential Role of Spin Fluctuations in High-T_c Superconductivity, Phys. Rev. Lett. **103**, 227001 (2009).
[10] S. Ideta, K. Takashima, M. Hashimoto, T. Yoshida, A. Fujimori *et al.*, Enhanced Superconducting Gaps in the Trilayer High-Temperature $Bi_2Sr_2Ca_2Cu_3O_{10+\delta}$ Cuprate Superconductor, Phys. Rev. Lett. **104**, 227001 (2010).
[11] S. Kunisada *et al.*, Observation of Bogoliubov Band Hybridization in the Optimally Doped Trilayer $Bi_2Sr_2Ca_2Cu_3O_{10+\delta}$, Phys. Rev. Lett. **119**, 217001 (2017).
[12] J. A. Slezak, J. Lee, M. Wang, K. McElroy, K. Fujita, B. M. Andersen, P. J. Hirschfeld, H. Eisaki, S. Uchida, and J. C. Davis, Imaging the impact on cuprate superconductivity of varying the interatomic distances within individual crystal unit cells, Proc. Natl. Acad. Sci. U.S.A. **105**, 3203 (2008).

[13] C. T. Lin and B. Liang, Growth of a hard-grown single crystal $Bi_2Sr_2Ca_2Cu_3O_{10+\delta}$, in *New Trends in Superconductivity, Proceedings of the NATO Advanced Research Workshop on New Trends in Superconductivity*, edited by J. F. Annett and S. Kruchinin (Kluwer Academic, Yalta, Ukraine, 2001), p. 19.

[14] B. Liang, C. Bernhard, T. Wolf, and C. T. Lin, Phase evolution, structural and superconducting properties of Pb-free $Bi_2Sr_2Ca_2Cu_3O_{10+\delta}$ single crystals, Supercond. Sci. Technol. **17**, 731 (2004).

[15] C. Ye, P. Cai, R. Yu, X. Zhou, W. Ruan, Q. Liu, C. Jin, and Y. Wang, Visualizing the atomic-scale electronic structure of the $Ca_2CuO_2Cl_2$ Mott insulator, Nat. Commun. **4**, 1365 (2013).

[16] T. Fujii, I. Terasaki, T. Watanabe, and A. Matsuda, Doping dependence of anisotropic resistivities in the trilayered superconductor $Bi_2Sr_2Ca_2Cu_3O_{10+\delta}$, Phys. Rev. B **66**, 024507 (2002).

[17] A. Piriou, Y. Fasano, E. Giannini, and Ø. Fischer, Effect of oxygen-doping on $Bi_2Sr_2Ca_2Cu_3O_{10+\delta}$ vortex matter: Crossover from electromagnetic to Josephson interlayer coupling, Phys. Rev. B **77**, 184508 (2008).

[18] C. Howald, P. Fournier, and A. Kapitulnik, Inherent inhomogeneities in tunneling spectra of $Bi_2Sr_2CaCu_2O_{8-x}$ crystals in the superconducting state, Phys. Rev. B **64**, 100504(R) (2001).

[19] K. M. Lang, V. Madhavan, J. E. Hoffman, E. W. Hudson, H. Eisaki, S. Uchida, and J. C. Davis, Imaging the granular structure of high-Tc superconductivity in underdoped $Bi_2Sr_2CaCu_2O_{8+\delta}$, Nature (London) **415**, 412 (2002).

[20] See Supplemental Material at http://link.aps.org/supplemental/10.1103/PhysRevLett.124.047003 for more detailed information.

[21] D. L. Feng *et al.*, Signature of superfluid density in the single-particle excitation spectrum of $Bi_2Sr_2CaCu_2O_{8+\delta}$, Science **289**, 277 (2000).

[22] I. Zeljkovic, Z. J. Xu, J. S. Wen, G. D. Gu, R. S. Markiewicz, and J. E. Hoffman, Imaging the impact of single oxygen atoms on superconducting $Bi_{2+y}Sr_{2-y}CaCu_2O_{8+x}$, Science **337**, 320 (2012).

[23] I. Zeljkovic *et al.*, Nanoscale interplay of strain and doping in a high-temperature superconductor, Nano Lett. **14**, 6749 (2014).

[24] R. Sekine, K. Ogata, A. Tsukada, and N. Miyakawa, Two sizes of superconducting gaps on an under-doped $Bi_{2.1}Sr_{1.9}Ca_2Cu_3O_{10+\delta}$ with $T_c \sim 101$ K by tunneling spectroscopy, Phys. Procedia **58**, 82 (2014).

[25] J. Nieminen, I. Suominen, R. S. Markiewicz, H. Lin, and A. Bansil, Spectral decomposition and matrix element effects in scanning tunneling spectroscopy of $Bi_2Sr_2CaCu_2O_{8+\delta}$, Phys. Rev. B **80**, 134509 (2009).

[26] A. Yamamoto, M. Onoda, E. Takayama-Muromachi, F. Izumi, T. Ishigaki, and H. Asano, Rietveld analysis of the modulated structure in the superconducting oxide $Bi_2(Sr, Ca)_3Cu_2O_{8+\delta}$, Phys. Rev. B **42**, 4228 (1990).

[27] B. M. Andersen, P. J. Hirschfeld, and J. A. Slezak, Superconducting gap variations induced by structural supermodulation in $Bi_2Sr_2CaCu_2O_8$, Phys. Rev. B **76**, 020507(R) (2007).

[28] K.-Y. Yang, T. M. Rice, and F.-C. Zhang, Effect of superlattice modulation of electronic parameters on the density of states of cuprate superconductors, Phys. Rev. B **76**, 100501(R) (2007).

[29] Y. He, S. Graser, P. J. Hirschfeld, and H. P. Cheng, Supermodulation in the atomic structure of the superconductor $Bi_2Sr_2CaCu_2O_{8+x}$ from ab-initio calculations, Phys. Rev. B **77**, 220507(R) (2008).

[30] C. Guo, H. F. Tian, H. X. Yang, B. Zhang, K. Sun, X. Sun, Y. Y. Peng, X. J. Zhou, and J. Q. Li, Direct visualization of soliton stripes in the CuO_2 plane and oxygen interstitials in $Bi_2(Sr_{2-x}La_x)CuO_{6+\delta}$ superconductors, Phys. Rev. Mater. **1**, 064802 (2017).

[31] W.-G. Yin and W. Ku, Tuning the in-plane electron behavior in high-Tc cuprate superconductors via apical atoms: A first-principles Wannier-states analysis, Phys. Rev. B **79**, 214512 (2009).

[32] M. Mori, G. Khaliullin, T. Tohyama, and S. Maekawa, Origin of the Spatial Variation of the Pairing Gap in Bi-Based High Temperature Cuprate Superconductors, Phys. Rev. Lett. **101**, 247003 (2008).

[33] E. Pavarini, I. Dasgupta, T. Saha-Dasgupta, O. Jepsen, and O. K. Andersen, Band-Structure Trend in Hole-Doped Cuprates and Correlation with $T_{c\,\max}$, Phys. Rev. Lett. **87**, 047003 (2001).

[34] H. Eisaki, N. Kaneko, D. L. Feng, A. Damascelli, P. K. Mang, K. M. Shen, Z. X. Shen, and M. Greven, Effect of chemical inhomogeneity in bismuth-based copper oxide superconductors, Phys. Rev. B **69**, 064512 (2004).

[35] S. Iwai, H. Mukuda, S. Shimizu, Y. Kitaoka, S. Ishida, A. Iyo, H. Eisaki, and S. I. Uchida, Imbalance of hole density between inner and outer planes and superconducting transition temperature in multilayered cuprates, JPS Conf. Proc. **1**, 012105 (2014).

[36] G. Vincini, K. Tanaka, T. Adachi, L. Sobirey, S. Miyasaka, S. Tajima, S. Adachi, N. Sasaki, and T. Watanabe, Double pair breaking peak in Raman scattering spectra of the trilayer cuprate $Bi_2Sr_2Ca_2Cu_3O_{10+z}$, Phys. Rev. B **98**, 144503 (2018).

[37] E. Berg, D. Orgad, and S. A. Kivelson, Route to high-temperature superconductivity in composite systems, Phys. Rev. B **78**, 094509 (2008).

[38] O. Yuli, I. Asulin, O. Millo, D. Orgad, L. Iomin, and G. Koren, Enhancement of the Superconducting Transition Temperature of $La_{2-x}Sr_xCuO_4$ Bilayers: Role of Pairing and Phase Stiffness, Phys. Rev. Lett. **101**, 057005 (2008).

[39] K. McElroy, D. H. Lee, J. E. Hoffman, K. M. Lang, J. Lee, E. W. Hudson, H. Eisaki, S. Uchida, and J. C. Davis, Coincidence of Checkerboard Charge Order and Antinodal State Decoherence in Strongly Underdoped Superconducting $Bi_2Sr_2CaCu_2O_{8+\delta}$, Phys. Rev. Lett. **94**, 197005 (2005).